Complete characterisation of a $(Sb_2O_3)_n$/SWNT inclusion composite

© S. Friedrichs, R.R. Meyer*, J. Sloan, A.I. Kirkland*, J.L. Hutchison**, M.L.H. Green

Wolfson Catalysis Centre (Carbon Nanotechnology Group), Inorganic Chemistry Laboratory,
Oxford OX1 3QR, U.K.
* Department of Materials Science,
Cambridge CB2 3QZ, U.K.
** Department of Materials,
Oxford OX1 3PH, U.K.

The detailed inclusion crystallography of a 1-dimensional valentinite Sb_2O_3 crystal incorporated within a helical (21,-8) single walled carbon nanotube has been identified from a phase image that was recovered via a modified object wave restoration scheme. A detailed analysis of asymmetric fringe contrast in the tube walls has provided strong evidence for the chiral sence of the tube itself. Due to the good agreement of observed wall periodicity with the determined absolute focus values and power spectra obtained from single-pixel line traces along both tube walls, we were able to determine the chiral sence of the SWNT and the tilt angle of the Sb_2O_3/SWNT composite relative to the electron beam. The angle between the optimum $\langle 1\ 0\ -1\rangle$ viewing direction of the crystal fraction and the tube axis, which is aligned with the $\langle 4\ -1\ 2\rangle$ direction of the Sb_2O_3 crystal, is 78.3°. Since small deviations from this viewing direction make an insignficant difference to the observed contrast, a tube inclination of 15° is plausible for both the Sb_2O_3 crystal and the assigned $(21, -8)$ SWNT, which is the mirror image of a $(13, 8)$ SWNT.

We acknowledge the Petroleum Research Fund, administered by the American Chemical Society (Grant N 33765-AC5), the EPSRC (Grant Nos GR/L59238 and GR/L22324) and Colebrand Ltd. for financial support. S.F. is indebted to BMBF and Fonds der Chemischen Industrie for additional financial support. J.S. is indebted to the Royal Society.

A modified object wave restoration scheme was used to recover the phase image of a Sb_2O_3 valentinite nanocrystal encapsulated within a single-walled carbon nanotube (SWNT) [1]. Within the nanocrystal, the atomic thickness in projection of individual antimony columns was determined and a substantial lattice contraction of the crystal along the tube axis observed. For the first time a detailed analysis of asymmetric fringe contrast in the tube walls has provided strong evidence for the chiral conformation of the nanotube itself.

SWNTs were produced using a metal catalysed arc synthesis similar to the method previously reported [2] and filled using Puratonic Sb_2O_3 (ALFA, 99.999%) according to the capillary technique described [3]. The product mixture was ground, dispersed in Analar pentane, placed onto a holey carbon support film and examined at 300 kV in a JEOL JEM-300F field emission gun transmission electron microscope (FEGTEM). The chemical identity of the filling material was confirmed using an energy dispersive X-ray microanalysis system (LINK "ISIS"). High resolution transition electron microscopy simulations, giving the complex wave function of the previously modelled objects, were performed using a standard multislice algorithm [4,5] utilising a code provided by Kirkland [6]. Atomic coordinates for (n, m) nanotubes were generated by mapping the strip $\{\mathbf{r}|0 \le \mathbf{r}\cdot\mathbf{C}_h < |\mathbf{C}_h|^2\}$ of a planar hexagonal graphene lattice (with a carbon–carbon distance $d_{C-C} = 1.44$ nm and lattice vectors $\mathbf{a}_1$, $\mathbf{a}_2$) onto a cylinder surface (Fig. 1). The integers (n, m) with $n > 0$ and $-n/2 < m \le n$ [7] uniquely define the structure of the nanotube *via* the chiral vector $\mathbf{C}_h = n\mathbf{a}_1 + m\mathbf{a}_2$ [8]. The special cases $(n, 0)$ and (n, m) represent the non-chiral "zigzag" and "armchair" configurations, respectively, while all other (n, m) nanotubes are chiral with $(n+m, -m)$ being the mirror image of (n, m).

The coordinates for the encapsulated Sb_2O_3 crystal were initially determined from a crystal fragment generated from the published valentinite structure of Sb_2O_3 [9].

Fig. 1 illustrates the relationship between the observed wall periodicity, nanotube conformation and tilt angle β for structure models and corresponding simulations of SWNTs with diameters close to that of the imaged 1.45 nm diameter SWNT, i.e. for a $(10, 10)$ "armchair" SWNT (Fig. 1, *a*), a $(18, 0)$ "zigzag" SWNT (Fig. 1, *b*) and a chiral $(21, -8)$ SWNT (Fig. 1, *c*).

The illustration shows that the "centre-to-centre" spacings will not be resolvable in the armchair case, as the carbon separation is only 0.125 nm in projection and this distance will be reduced further as the tubule is tilted with respect to the image plane, causing the carbon atoms to stagger in projection. In the case of an untilted zigzag tubule (Fig. 1, *b*), both carbon walls are clearly visible as they have a separation of 0.216 nm in projection (Fig. 1, *b*, left). As the tubule is tilted, the simulated wall spacings smear as the carbon zigzags start to stagger in projection. For both non-chiral tubules, the contrast will still be equal on both walls as the tube is tilted. A chiral tube (e.g. Fig. 1, *c*), however, will display resolvable contrast on one tube wall if the difference $\delta = |\alpha \pm \beta|$ is small, where $\alpha = \angle(\mathbf{C}_h, \mathbf{a}_1) = \arctan\left(\sqrt{3}\,m/(2n+m)\right)$ is the chiral angle and the angle β is the tilt angle between the tube axis and the image plane. β is defined as positive if the top end of the tube is above the plane, as for this specimen.

Fig. 2, *a* shows the restored phase image of a 1.45-nm-diameter SWNT containing an encapsulated single crystal of

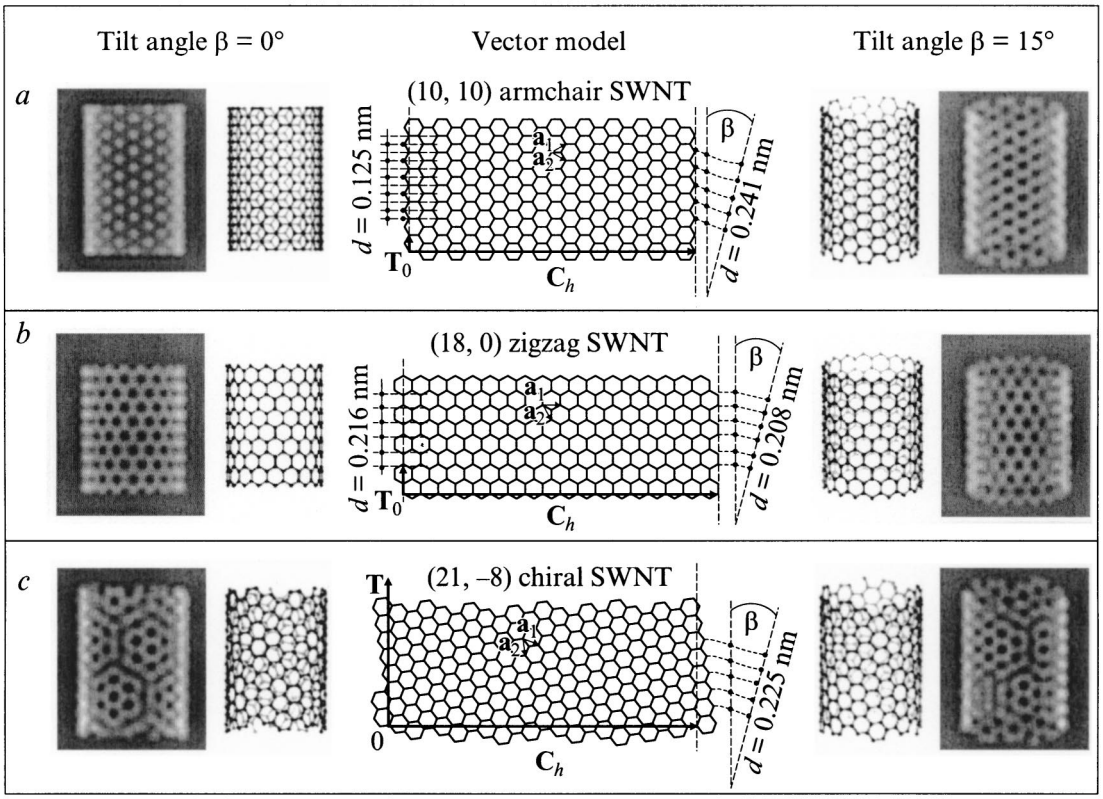

Figure 1. Schematic illustration of the observable resolution of SWNT walls, depending on the their classification and the tilt angle β. The visible appearance of carbon–carbon spacings in the walls of a $(10, 10)$ armchair, a $(18, 0)$ zigzag and a $(21, -8)$ chiral tube are explained respectively. The middle column shows the unrolled honeycomb lattice of a nanotube, illustrating the chiral vector $\mathbf{C}_h$ and the translation vector $\mathbf{T}$, which define the rolling of the graphene sheet to give a nanotube of a specific classification and diameter $(\mathbf{T}[(10, 10)] = (1, -1); \mathbf{T}[(18, 0)] = (1, -2); \mathbf{T}[(21, -8)] = (5, -34)$). $\mathbf{a}_1$ and $\mathbf{a}_2$ are the unit vectors. The rectangle bounded by the thin dashed lines and the chiral vector, marks the unit cell (note: the unit cell of the $(21, -8)$ SWNT is only partially displayed). The columns adjacent to the illustrated graphene sheet display modelled fractions of the SWNTs, parallel to the image plane (i.e.: tilt angle $\beta = 0°$; left column) and tilted by $\beta = 15°$ out of the image plane (right column). The two outer columns show simulated phase images of the displayed models.

Sb_2O_3, for each of which, an individual absolute defocus level was determined independently. Recombination of the absolute defocus levels along the tube revealed that the imaged composite is inclined by a tilt angle of $\beta = 17 \pm 5°$ with respect to the image plane, with the top end of the tube higher in the beam path.

The phase image in Fig. 2, *a* displays a periodic lattice spacing of 0.224 ± 0.04 nm along the right wall of the SWNT, whereas the contrast variations on the left wall are effectively random. The observed periodic spacing on the right wall corresponds to the centre-to-centre spacing ($1.5d_{C-C} = 0.216$ nm) between neighbouring zigzag rows of carbon atoms in the SWNT wall lattice, when viewed in projection. This indicates that the imaged tube is chiral with a negative chiral angle α and hence a negative integer m. As the number of atoms in projection on the tube wall is small, strong contrast will be visible for values for δ of up to 10°, and the observed spacing is given by $1.5d_{C-C} \cos\beta / \cos\alpha$ as we can see for the modelled $(21, -8)$ SWNT in Fig. 1, *c*.

The phase image and corresponding line profiles in Fig. 2, *a* can best be matched to an approximate $\langle 1\ 0\ -1 \rangle$ projection through a fragment of Sb_2O_3 derived from the orthorhombic polymorph valentinite form, which consists of infinite double chains of SbO_3 units, as opposed to the cubic senarmonite form, consisting of molecular units of Sb_4O_6 [10]. The proposed structure model is shown in Fig. 2, *c*, together with an end-on view of the Sb_2O_3/SWNT composite (Fig. 2, *d*). A corresponding simulated phase image is given in Fig. 2, *b*.

The white spots in the reconstructed phase correspond to projection through atomic columns of antimony only. The oxygen sublattice could not be resolved due to the weak scattering properties of oxygen atoms, their staggered positions in projection, and the limited resolution (*ca.* 0.16 nm) present in the restoration. Comparison of multislice simulations of the restored phase of Sb_2O_3 lattice fractions of appropriate thickness with equivalent simulated antimony sublattice fractions confirmed that the phase contrast due to the oxygen sublattice is negligible compared to that due to the antimony sublattice.

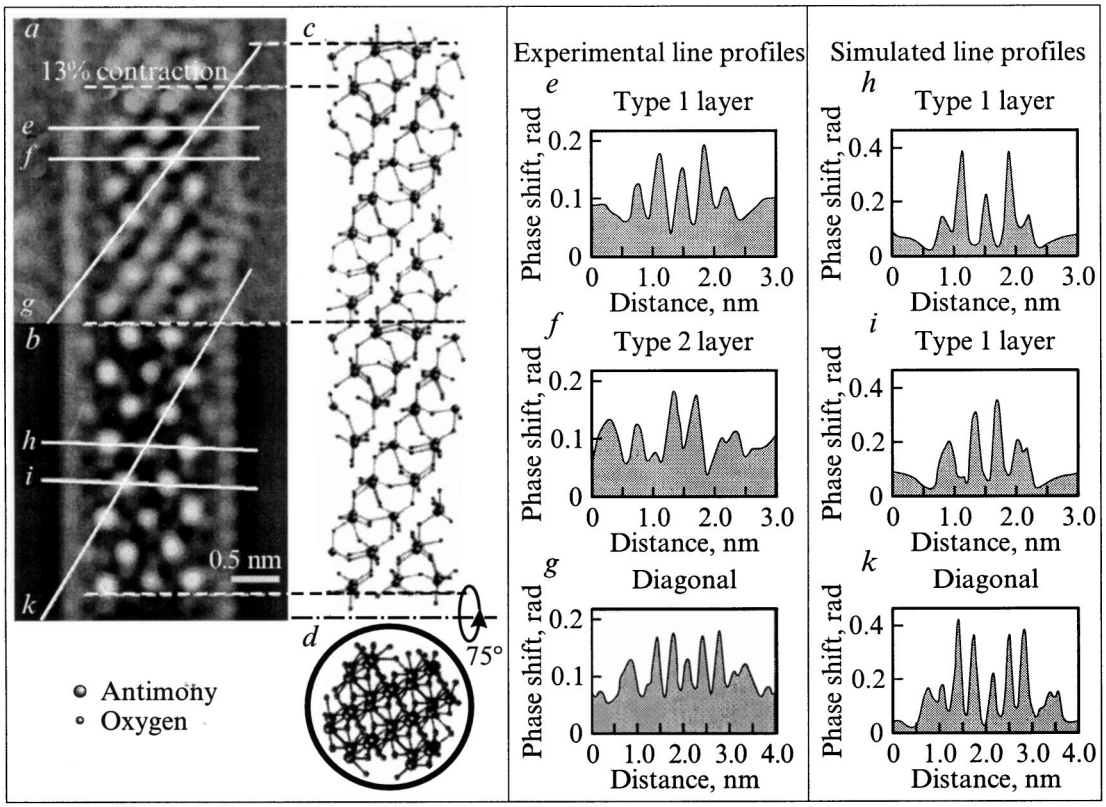

Figure 2. Composite diagram showing the experimental restored phase image (a), the simulated phase image (b), and the structural model in the observed orientation (c) and in end-on view (d). The white lines mark single-pixel line profiles through the experimental phase image (e–g) and through the simulated phase image (h–k).

In the bulk valentinite structure, the Sb_2O_3 double chains run parallel to $\langle 0\ 0\ 1\rangle$ with each antimony atom being coordinated by three oxygen atoms, and each Sb of the infinite SbO_3 chains being bridged by a shared oxygen [9]. In the case of the encapsulated crystal, the $\langle 4\ -1\ 2\rangle$ direction of the Sb_2O_3 crystal is aligned along the tube axis which has a tilt angle of 78.3° with respect to the optimum $\langle 1\ 0\ -1\rangle$ viewing direction. Small deviations from this viewing direction make an insignificant difference to the observed contrast and hence a tube inclination of 15° was used for the simulated object (Fig. 2, b), in order to account for the observed contrast within the tube wall. The same inclination angle was applied to the model shown in Fig. 2, c.

The repeating structural motif of the imaged encapsulated Sb_2O_3 crystal can be described as a repeating sequence of a layer (type 1 layer) containing three columns of antimony atoms followed by a layer (type 2 layer) containing two columns of antimony atoms arranged perpendicular to the tube axis. In the structure model, we assume coordination appropriate for the bulk valentinite structure. Within each type 1 or type 2 layer, the intensities of the peaks corresponding to individual Sb columns vary in a complex fashion. The line profile across a type 1 layer shows a stacking pattern of 3–2–3 Sb atoms in projection (Fig. 2, e). By contrast the line profile across a type 2 layer gives two peaks of equal intensity (Fig. 2, f), approximately equivalent to the higher peak within the type 1 layer, indicating Sb columns of three atoms in thickness. These observations lead to the modelled Sb_2O_3 crystal fragment, which has sequences of 3–2–3 and 3–3 layers with a fourfold repeat period along the $\langle 4\ -1\ 2\rangle$ direction (Fig. 2, c).

Comparison with the equivalent line profiles through the simulated image support the interpretation of the observed Sb_2O_3/SWNT composite.

Since the oxygen sublattice could not be resolved the oxygen coordination is predicted from the bulk valentinite structure. In order to fit the modelled Sb_2O_3 crystal into the 1.45-nm-diameter SWNT therefore, some oxygen atoms on the surface of the crystal were omitted. This can be justified in terms of the reduction in coordination that will be expected at the Sb_2O_3/SWNT interface (*cf.* 2×2 and 3×3 KI crystals formed within SWNT [11,12]).

The multislice simulation in Fig.2, b also shows weak contrast close to the tube walls, indicating the presence of single atom columns at the edge of the encapsulated valentinite crystal fragment, as visible in Fig. 2, c. The corresponding experimental phase image also shows evidence for additional weak peaks at some of these sites, possibly caused by individual Sb atoms. However, the intensities of these peaks are sufficiently close to the background noise levels that it is impossible to definitely assing these contrasts to such single atoms without a more accurate analysis of the phase shift.

Significant lattice distortions were observed in the Sb_2O_3 crystal encapsulated within the (21, −8) SWNT. In comparison with the bulk structure of valentinite, the encapsulated crystal shows a longitudinal contraction of 13% along the $\langle 4{-}1\ 2\rangle$ axis. This contraction occurs in a similar fashion but is relatively larger than that which we reported for the SWNT encapsulated KI 3×3 crystal [11]. Direct lattice measurements from line traces, show an average spacing of ~ 0.552 nm between two type 1 layers or two type 2 layers respectively, whereas in the simulated phase image (based on the Sb positions in bulk valentinite) equivalent layers are spaced at average intervals of ~ 0.638 nm. The observed lattice contraction may be caused by an interaction between the Sb_2O_3 crystal and the SWNT walls and it may be partially caused by the reduction in coordination at the Sb_2O_3/SWNT interface.

We thank the Department of Materials Science and Metallurgy, Cambridge for the provision of computational facilities.

References

[1] S. Friedrichs, R.R. Meyer, J. Sloan, A.I. Kirkland, J.L. Hutchinson, M.L.H. Green. Phys. Rev. B, in print.
[2] C. Journet, W.K. Maser, P. Bernier, A. Loiseau, M.L. Delachapelle, S. Lefrant, P. Deniard, R. Lee, J.E. Fisher. Nature (Lond.) **388**, 756 (1997).
[3] J. Sloan, D.M. Wright, H.-G. Woo, S. Bailey, G. Brown, A.P.E. York, K.S. Coleman, J.L. Hutchison, M.L.H. Green. Chem. Commun. 699 (1999).
[4] J.M. Cowley, A.F. Moodie. Acta. Cryst. **10**, 609 (1957).
[5] P. Goodman, A.F. Moodie. Acta. Cryst. **A30**, 280 (1974).
[6] E.J. Kirkland. In: Advanced Computing in Electron Microscopy. Plenum Press. N. Y. (1998).
[7] The lower limit for m used here differs from the definition given in Ref. [8], to ensure that the chiral angle α lies in the range $-30 < \alpha \leq 30^\circ$.
[8] R. Saito, C. Dresselhaus, M.S. Dresselhaus. Physical Properties of Carbon Nanotubes. Imperial College Press, London (1998).
[9] C. Svensson. Acta Cryst. **B30**, 458 (1974).
[10] C. Svensson. Acta Cryst. **B31**, 2016 (1975).
[11] R.R. Meyer, J. Sloan, R.E. Dunin-Borowski, A.I. Kirkland, M.C. Novotny, S.R. Bailey, J.L. Hutchison, M.L.H. Green. Science **289**, 1324 (2000).
[12] If the K and I atoms are superposed in projection as in the case of a crystal viewed along $\langle 100\rangle$, for example, then the resulting image contrast from both columns is summed in projection as we reported for a 2×2 KI crystal formed inside a SWNT. [J. Sloan et al. Chem. Phys. Lett. **329**, 61 (2000).]